



A Journal of the Gesellschaft Deutscher Chemiker

# Angewandte Chemie

GDCh

International Edition

www.angewandte.org

## Accepted Article

**Title:** Catalytic production of alanine from waste glycerol

**Authors:** Yunzhu Wang, Shinya Furukawa, Song Song, Qian He, Hiroyuki Asakura, and Ning Yan

This manuscript has been accepted after peer review and appears as an Accepted Article online prior to editing, proofing, and formal publication of the final Version of Record (VoR). This work is currently citable by using the Digital Object Identifier (DOI) given below. The VoR will be published online in Early View as soon as possible and may be different to this Accepted Article as a result of editing. Readers should obtain the VoR from the journal website shown below when it is published to ensure accuracy of information. The authors are responsible for the content of this Accepted Article.

**To be cited as:** *Angew. Chem. Int. Ed.* 10.1002/anie.201912580  
*Angew. Chem.* 10.1002/ange.201912580

**Link to VoR:** <http://dx.doi.org/10.1002/anie.201912580>  
<http://dx.doi.org/10.1002/ange.201912580>

## COMMUNICATION

## Catalytic production of alanine from waste glycerol

Yunzhu Wang, Shinya Furukawa, Song Song, Qian He, Hiroyuki Asakura and Ning Yan\*

**Abstract:** Chemical synthesis of amino acids directly from biomass feedstock is rare. Herein, we report a one-step protocol to convert crude glycerol from the biodiesel industry into 43% alanine over a Ru<sub>1</sub>Ni<sub>7</sub>/MgO catalyst. The multifunctional catalytic system promotes glycerol conversion into lactic acid, and then to alanine. X-ray absorption spectroscopy and scanning transmission electron microscopy revealed the existence of bimetallic RuNi species, whereas density functional theory calculations suggested Ni-doped Ru substantially decreased the  $E_a$  of C–H bond dissociation of lactate alkoxide to form pyruvate, which is the rate-determining step. The catalytic route established in this work creates new opportunities for glycerol utilization and enriches the substrate scope of renewable feedstock to access value-added amino acids.

Glycerol is the major by-product in biodiesel industry soon reaching an annual scale of 3.7 million metric tons.<sup>[1]</sup> Glycerol on its own is a low-value chemical whose production far exceeds the current demand. Extensive research activities have been devoted to converting glycerol to value-added chemicals, following oxidation/dehydrogenation, dehydration, hydrogenolysis, steam reforming and transesterification pathways.<sup>[2]</sup> In the oxidation pathway, glycerol can be converted into tartronic acid, glyceric acid, dihydroxyacetone or others depending on the regioselectivity and/or degree of oxidation.<sup>[3]</sup> The dehydration pathway is useful to generate C=C bond-containing chemicals such as acrolein.<sup>[1a]</sup> Hydrogenolysis is applied to partially or fully remove oxygen from glycerol, offering propanediols, propanols, propylene glycol, et al. as products.<sup>[4]</sup> Chemicals with more complex functionalities, such as lactic acid, may be produced when two or more catalytic functionalities are introduced into the same catalyst.<sup>[5]</sup>

All the strategies mentioned above only offer oxygen-containing chemicals from glycerol. Converting glycerol to organonitrogen chemicals, which often have higher commercial value,<sup>[6]</sup> has received much less attention. Limited reports either

used organic amines as the nitrogen source, or suffered from various other issues such as low selectivity and/or the requirement of multiple steps.<sup>[7]</sup> Recently, transformation of biomass-derived hydroxyl acids into corresponding amino acids has been reported, opening a path towards amino acids.<sup>[8]</sup> Considering that the conversion of glycerol to lactic acid<sup>[5]</sup> and the conversion of lactic acid to alanine<sup>[8a]</sup> have both been achieved, an opportunity arise to combine the two steps in a single catalytic system comprising both base and metal functionalities so that glycerol is directly converted into alanine (Figure 1). A major challenge of the new route is the identification of proper catalytic systems that enable efficient, sequential dehydrogenation, dehydration, rearrangement, and amination steps.



**Figure 1.** An illustration of one-step conversion of waste glycerol to alanine.

Initially, a standard 2 wt% Ru/MgO catalyst, prepared by co-precipitation (CP) method followed by calcination in air and reduction in H<sub>2</sub> both at 500 °C, was used in conversion of glycerol (Table S1). Little alanine (0.7%) was observed in the presence of NaOH and 10 bar H<sub>2</sub> at 220 °C for 4 h (Figure 2a). Then, a series of bimetallic Ru<sub>1</sub>M<sub>10</sub>/MgO (M = Fe, Co, Ni and Zn) catalysts were prepared using the CP method, with Ru to second metal molar ratio fixed at 1:10 (denoted as Ru<sub>1</sub>M<sub>10</sub>/MgO, Table S1). A general trend is that the Ru<sub>1</sub>M<sub>10</sub>/MgO catalysts exhibited much-improved activity than the single-metallic Ru/MgO catalyst. In particular, Ru<sub>1</sub>Ni<sub>10</sub>/MgO offered 48 times more alanine (34%) than Ru/MgO under the same condition. Of note, pure Ni catalysts, such as Ni/MgO (20 wt%) and Raney® Ni presented essentially no activity towards alanine, indicating Ru, instead of Ni, is the main catalytically active species.

A series of Ru<sub>1</sub>Ni<sub>10</sub> catalysts supported on MgO, CNT, TiO<sub>2</sub> and CeO<sub>2</sub> using wet-impregnation (W) method, and ZnO and Al<sub>2</sub>O<sub>3</sub> using CP method were prepared and evaluated. Despite being slightly less effective than the CP-derived Ru<sub>1</sub>Ni<sub>10</sub>/MgO catalyst, Ru<sub>1</sub>Ni<sub>10</sub>/MgO-W and Ru<sub>1</sub>Ni<sub>10</sub>/CNT-W were much better than catalysts on other supports (Figure 2b). Considering MgO and CNT are stable under highly basic conditions while others are not, the observed support effect is attributed to the support stability under the reaction conditions. As the Ni:Ru ratio increased from 3 to 7 on MgO using CP method (Table S2), the alanine yield increased gradually to 36%. Meanwhile, the lactic acid yield displayed a reversed trend decreasing from 26% to 10% (Figure 2c). Further increasing the Ni:Ru ratio to 10 did not induce a significant increase in alanine yield. Within the first 0.5 h over the optimum Ru<sub>1</sub>Ni<sub>7</sub>/MgO catalyst (reduced at 600 °C, as discussed below), lactic acid was rapidly produced reaching 71%

[\*] Dr. Y. Wang, Dr. S. Song, Prof. Dr. N. Yan  
Department of Chemical and Biomolecular Engineering  
National University of Singapore  
4 Engineering Drive 4, Singapore 117585, Singapore  
E-mail: [ning.yan@nus.edu.sg](mailto:ning.yan@nus.edu.sg)  
Prof. Dr. S. Furukawa  
Institute for Catalysis, Hokkaido University, N-21, W-10, Sapporo  
001-0021, Japan.  
Elements Strategy Initiative for Catalysis and Battery, Kyoto  
University, Kyoto Daigaku Katsura, Nishikyo-ku, Kyoto, Japan, 615-  
8510.  
Prof. Dr. Q. He,  
Department of Materials Science and Engineering  
National University of Singapore  
9 Engineering Drive 1, Singapore 117575, Singapore  
Prof. Dr. H. Asakura  
Department of Molecular Engineering, Graduate School of  
Engineering, Kyoto University, Kyotodaijaku Katsura, Nishikyo-ku,  
Kyoto 615-8510, Japan  
Supporting information for this article is given via a link at the end of  
the document.

## COMMUNICATION

yield, whereas alanine yield was only 4.5% with small amount of glycine detected (Figure 2d and Table S3). The alanine yield progressively increased to 45% in the next 3.5 h, together with the declining yield of lactic acid to less than 17%. These observations are in line with the designed two-step strategy in which lactic acid is the key intermediate. Below 200 °C the activity is very low whereas at 240 °C or above, side-reactions become significant (Figure S1).

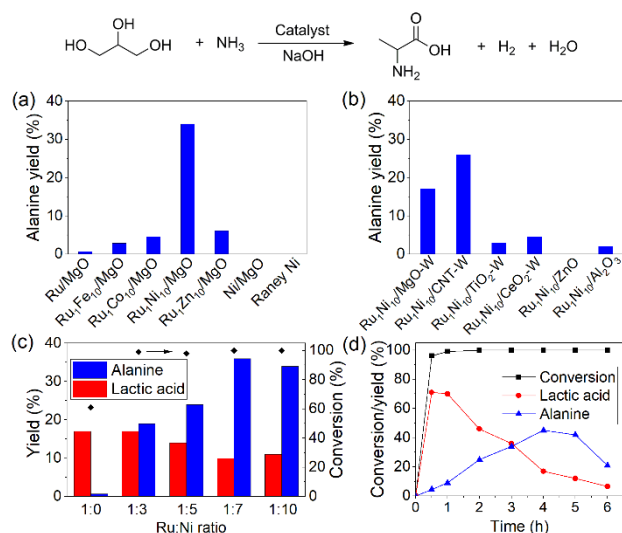


**Figure 2.** Catalytic conversion of glycerol to alanine in a batch reactor over (a) Ru<sub>1</sub>M<sub>10</sub>/MgO, Ru/MgO, Ni/MgO and Raney® Ni catalysts, (b) Ru<sub>1</sub>Ni<sub>10</sub> on different supports (W indicates catalysts prepared by wet-impregnation method), (c) MgO supported RuNi<sub>x</sub> catalyst with varied Ru:Ni ratio, and (d) conversion/yield profile of Ru<sub>1</sub>Ni<sub>7</sub>/MgO catalyst as a function of time. Reaction conditions: 100 mg glycerol, 200 mg NaOH, 67 mg catalysts or 30 mg Raney® Ni (Ru:substrate molar ratio = 0.012), 2 mL NH<sub>3</sub>H<sub>2</sub>O (25 wt%), 10 bar H<sub>2</sub>, 220 °C, 4 h. Catalysts were reduced at 500 °C for (a-c) and 600 °C for (d).

The effect of calcination temperature in the range of 300 °C to 900 °C was investigated (Figure S2). As suggested by X-ray powder diffraction (XRD) analysis (Figure S3), 500 °C is the minimum temperature required for the complete generation of MgO from its precursor. H<sub>2</sub>-temperature programmed reduction (H<sub>2</sub>-TPR) profiles of the Ru<sub>1</sub>Ni<sub>7</sub>/MgO and Ru/MgO catalysts exhibited reduction peaks at around 450-475 °C (Figure S4). Correspondingly, the alanine yield has a positive correlation with the catalyst reduction temperature in the range of 300 °C to 600 °C, hinting that the metallic species are the active sites (Figure S5). From these studies, 500 °C and 600 °C were selected as calcination and reduction temperature, respectively.

X-ray absorption near edge structure (XANES) revealed that the valent state of Ru in Ru/MgO is between Ru<sup>4+</sup> (RuO<sub>2</sub> as reference) and Ru<sup>0</sup> (Ru foil as reference) (Figure 3a). With addition of Ni, the K-edge absorption of Ru in Ru<sub>1</sub>Ni<sub>7</sub>/MgO exhibited a red-shift towards that of the metallic Ru. X-ray photoelectron spectroscopy (XPS) provided similar information that Ru in Ru<sub>1</sub>Ni<sub>7</sub>/MgO is closer to metallic state than in Ru/MgO (Figure S6a). In both XPS and XANES, Ni is oxidized due to the exposure to air before measurements (Figure 3b and Figure S6b). Extended X-ray absorption fine structure (EXAFS) fitting results

of the Ru K-edge for Ru<sub>1</sub>Ni<sub>7</sub>/MgO suggested a Ru-Ni coordination number of 2.9, providing evidence of Ru-Ni alloy structure (Table S4 and Figure S7). Selected catalysts were also studied using aberration-corrected scanning transmission electron microscopy (STEM). Figure 3(c) shows a representative high angle annular dark-field (HAADF) image of the Ru<sub>1</sub>Ni<sub>7</sub>/MgO catalyst. From the atomic number (Z) contrast, metal particles less than 10 nm were found uniformly dispersed on the MgO support. The compositions of these particles were further studied using energy-dispersive X-ray spectroscopy (X-EDS). A representative HAADF image, the corresponding chemical map and elemental composition of selected area were shown in Figure 3(d), 3(e-f) and Figure S8 respectively, indicating that the nanoparticles are Ru-Ni alloys. Based on the evidence from XANES, XPS and STEM analysis, and the fact that NiO can be reduced to metallic Ni in the presence of Ru under the reaction condition (10 bar H<sub>2</sub> at 220 °C) owing to the hydrogen spillover capability of Ru to Ni,<sup>[9]</sup> we postulate bimetallic RuNi species to be the key for the exceptional activity.

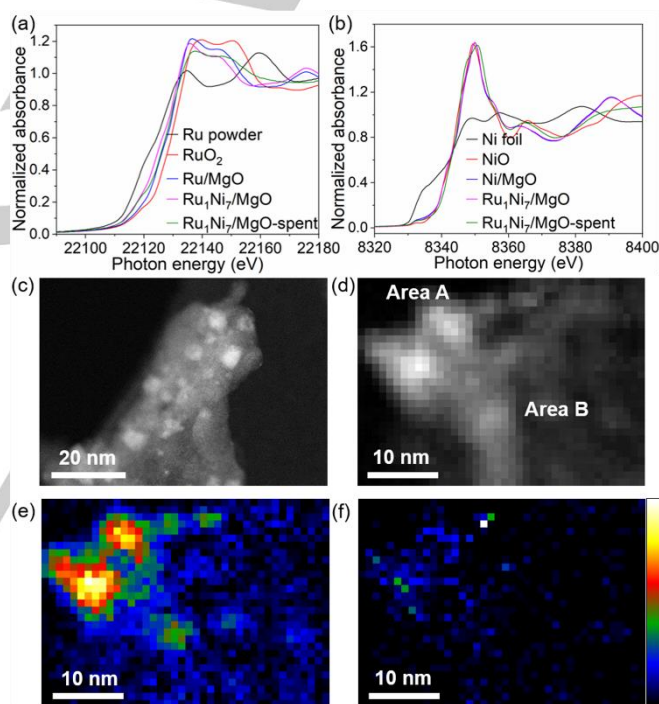


**Figure 3.** (a-b) XANES spectra of Ru<sub>1</sub>Ni<sub>7</sub>/MgO, Ru/MgO, Ni/MgO and Ru<sub>1</sub>Ni<sub>7</sub>/MgO-spent catalysts. (c) A representative HAADF image of Ru<sub>1</sub>Ni<sub>7</sub>/MgO catalyst, (d-f) EDS mapping of particles in the Ru<sub>1</sub>Ni<sub>7</sub>/MgO catalyst. The simultaneously obtained HAADF signal, Ni K-peak map and Ru L-peak map are shown in (d), (e) and (f) respectively.

<sup>13</sup>C nuclear magnetic resonance (NMR) spectrum of the product mixture using glycerol-<sup>13</sup>C<sub>3</sub> as the starting material was recorded. The spectra of the product mixture was relatively simple throughout the reaction duration of 1 h (Figure S9) or 4 h (Figure 4a). Lactic acid and alanine are the main species identified, substantiating lactic acid to be the only stable, abundant intermediate in the system. A small amount of C<sub>1</sub> (e.g. formic acid-<sup>13</sup>C and formamide-<sup>13</sup>C) and C<sub>2</sub> species (e.g. glyceric acid-<sup>13</sup>C<sub>2</sub>)

## COMMUNICATION

were detected, representing the only identifiable side reactions. Based on above and related studies in the literature,<sup>[10]</sup> a plausible reaction pathway is proposed (Figure 4b). Sequential dehydrogenation, dehydration and rearrangement lead to lactic acid from glycerol. Lactic acid then reacts with ammonia to form alanine following a dehydrogenation-amination-hydrogenation pathway.<sup>[8a]</sup> Hydrogenolysis of C<sub>3</sub> species into C<sub>1</sub> and C<sub>2</sub> products are the main side reactions. Metal and base act as active sites for dehydrogenation/hydrogenation/hydrogenolysis and dehydration/Cannizzaro reaction, respectively.<sup>[11]</sup> Base also promotes metal catalysed glycerol dehydrogenation by deprotonation,<sup>[12]</sup> and likely displaces lactic acid/alanine from catalyst surface as sodium lactate/sodium alaninate, which explains the proportional increase of lactic acid and alanine yields as a function of NaOH amount (Figure S10).

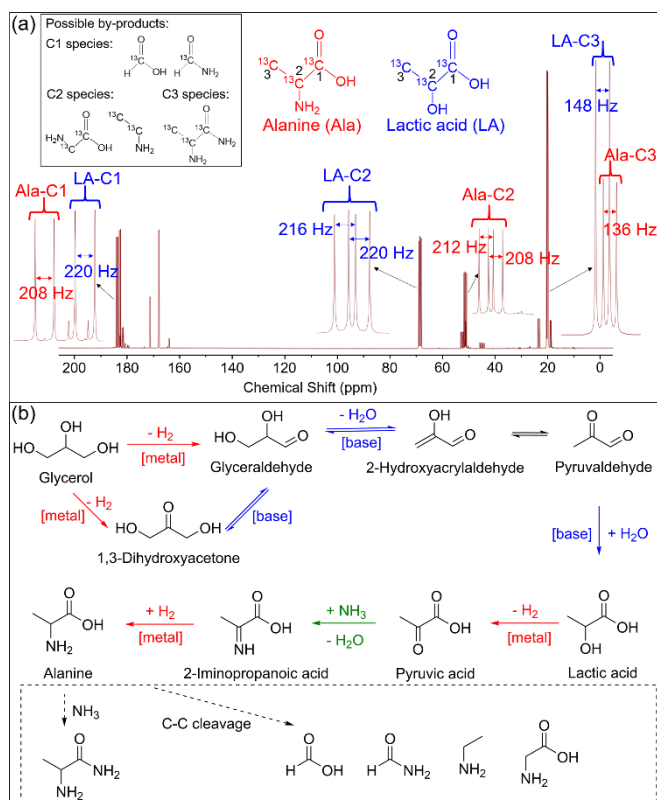


**Figure 4.** (a) <sup>13</sup>C NMR spectra of alanine and lactic acid produced from glycerol-<sup>13</sup>C<sub>3</sub>. Reaction condition: 108 mg glycerol-<sup>13</sup>C<sub>3</sub>, 67 mg Ru<sub>1</sub>Ni<sub>7</sub>/MgO, 200 mg NaOH, 2 mL NH<sub>3</sub>H<sub>2</sub>O (25 wt%), 10 bar H<sub>2</sub>, 220 °C, 4 h. (b) Proposed reaction network.

Conversion of glycerol to lactic acid (step I) and amination of lactic acid to alanine (step II) were evaluated separately over the Ru catalysts (Table 1). Step II is 5 times slower than step I over the Ru<sub>1</sub>Ni<sub>7</sub>/MgO catalyst under the same reaction condition. In fact, Ru<sub>1</sub>Ni<sub>7</sub>/MgO provided the highest rate in lactic acid amination (step II) that differentiated it from less active catalysts (Table S5). Considering C-H bond cleavage at α-carbon is the rate-determining step (r.d.s.) in lactic acid amination,<sup>[8a]</sup> and that amination is much slower than glycerol to lactic acid, C-H bond activation is the r.d.s. in glycerol transformation into alanine. A

physical mixture of Ru/MgO and Ni/MgO did not afford alanine with substantial yield, suggesting the importance of the existence of Ru and Ni in close proximity to promote C-H activation. Of note, the overall alanine production rate was lower than the lactic acid amination rate. A plausible explanation is that the unreacted glycerol inhibit lactic acid formation by strongly coordinate to the catalyst. Indeed, adding external glycerol decreased the alanine yield in lactic acid amination reaction (Table S5). Considering the conversion of glycerol is much faster over the RuNi catalyst (Figure 2d) than over the Ru catalyst (Figure S11), a second function of Ni in the system is to accelerate glycerol transformation into lactic acid although the underlying mechanism needs further exploration.

**Table 1.** Reaction rates of glycerol to alanine.<sup>[a]</sup>

Step	Substrate	Solvent	Time (h)	Conv. (%)	Yield (%)	Production rate <sup>[b]</sup> (mmol/g/h)
Over all	Glycerol	NH <sub>3</sub> H <sub>2</sub> O	0.67	15	0.12 <sup>[e]</sup>	0.19
I	Glycerol <sup>[c]</sup>	H <sub>2</sub> O	0.33	11	5.4 <sup>[f]</sup>	32
II	Lactic acid	NH <sub>3</sub> H <sub>2</sub> O	1	5.9	5.0 <sup>[e]</sup>	5.6
II	Lactic acid <sup>[d]</sup>	NH <sub>3</sub> H <sub>2</sub> O	3	6.8	6.2 <sup>[e]</sup>	2.2

[a] Reaction conditions: 100 mg substrate, 10 mg Ru<sub>1</sub>Ni<sub>7</sub>/MgO, 200 mg NaOH, 2 mL solvent, 10 bar H<sub>2</sub>, 220 °C. [b] Calculated by mmol of product (alanine or lactic acid) over gram of catalyst over time. [c] 5 mg Ru<sub>1</sub>Ni<sub>7</sub>/MgO. [d] 10 mg Ru/MgO. [e] Yield of alanine. [f] Yield of lactic acid.

Next, DFT study was conducted to further understand the role of Ni. We considered not only a standard flat slab surface but also interfacial models with a Ru<sub>20</sub> cluster on MgO(100) (Figure 5a). Two different metal-support interfaces were compared to consider the structural difference (Figure 5b, A and B sides). The activation and reaction energies ( $\Delta E$  and  $E_a$ , respectively) of the rate-determining step—C-H activation of lactate alkoxide to pyruvate—were calculated on various catalyst structures. For Ru<sub>20</sub>-MgO(100), the molecules were placed on the interface so that the alkoxide/carbonyl and carboxylate moieties bound to Ru (metal) and Mg (support), respectively. Based on the phase diagram of the Ru-Ni system, where only a small amount of Ni (<7%) can be dissolved into Ru,<sup>[13]</sup> one-atom substitution of Ru by Ni was considered. The position of Ru→Ni substitution was varied so that the Ni atom bound to different part of the molecules; alkoxide O (O<sub>al</sub>), secondary C (C<sub>2</sub>), eliminated H (H<sub>el</sub>), and carbonyl O (O<sub>ca</sub>, only for Ru(0001)) (Figure 5 and Figures S12-S21 for detailed structures). Ru-NiO interface was also considered by substituting two Mg cations of Ru<sub>20</sub>-MgO(100) by Ni.

Figure 5c summarizes the overall relationship between  $E_a$  and  $\Delta E$ . A rough linear correlation was observed, indicating that the reaction mainly follows the Bønsted-Evans-Polanyi principle. The interfacial sites (A and B) gave much lower  $E_a$  than the metallic terrace sites, probably because of the less atomic displacement during the C-H activation (Figures S12 and S15). Although these are only a part of numerous possible sites, the

## COMMUNICATION

metal–support interface is likely to work as an effective reaction site for the C–H activation of lactate. For the Ru<sub>20</sub>–MgO(100)A series, Ru→Ni substitution at O<sub>ai</sub> significantly lowered  $E_a$  (circles to triangles), while that at C<sub>2</sub> increased  $E_a$ . Similar trends were observed in other series (circles to squares), but there was no obvious trend for the substitution at H<sub>ei</sub> sites. These results indicate that the doped Ni in Ru facilitates the reaction when the alkoxide oxygen binds to Ni. On the contrary, Mg→Ni substitution (Figure 5c, filled to open symbols) did not show a specific trend, suggesting that Ru–NiO interface does not strongly contribute to the catalytic performance. Thus, the DFT study suggests the significant role of the Ru–Ni alloy phase on the enhanced catalysis, in agreement with the experimental observations (Figure 2c) that the major function of Ni is to promote Ru catalysed conversion of lactic acid to alanine.

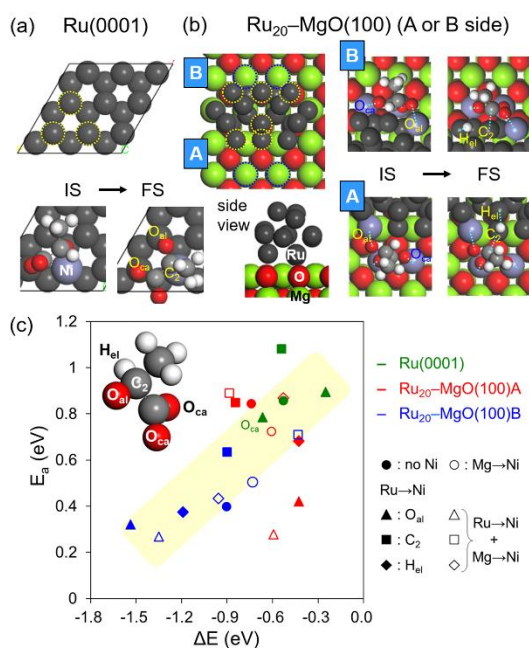


**Figure 5.** DFT calculations for C–H activation of lactate alkoxide over (a) Ru(0001) surface and (b) Ru<sub>20</sub>–MgO(100) interface with Ni-doping. Yellow and blue dotted circles indicate the position of Ni-substitution (yellow: at Ru binding to O<sub>ai</sub>, C<sub>2</sub>, H<sub>ei</sub>, O<sub>ca</sub>; blue: at Mg binding to O<sub>ca</sub>). Optimized structures of the initial (IS) and final states (FS) on (a) Ru(0001) (Ru→Ni at O<sub>ai</sub>) and (b) Ru<sub>20</sub>–MgO(100)A/B (Ru→Ni at O<sub>ai</sub> plus Mg→Ni) are also shown. Light blue dotted lines indicate chemical bond between Ru(Ni) and C, O, or H atom. (c) Relationship between  $E_a$  and  $\Delta E$  in C–H activation of lactate alkoxide over various Ru and Ru–Ni sites. Inset shows notation of the constituent atoms of lactate alkoxide.

Finally, we tested the effectiveness of the system in converting crude glycerol provided by Qingdao New Chemical Co., Ltd. (China) with 56% glycerol purity. Common impurities in waste glycerol include water, methanol, base and fatty acid salts. Under optimized conditions, 43% alanine was directly produced, indicating the robust activity of the Ru<sub>1</sub>Ni<sub>7</sub>/MgO catalyst. Catalyst recycling was conducted using crude glycerol as feedstock (Figure S22). Negligible activity loss was observed in the second cycle (40% yield), and some activity loss in the third run. The spent Ru<sub>1</sub>Ni<sub>7</sub>/MgO catalyst was characterized by XANES and

TEM analysis. The valence states of Ru and Ni were almost unchanged (Figure 3a–b) but the size of the NPs slightly increased (Figure S23), the latter of which might account for the loss of activity.

In summary, glycerol has been converted in a single-step to alanine over a RuNi bimetallic catalyst in aqueous ammonia. Lactic acid was determined as the key intermediate, and the amination of lactic acid to alanine was the rate-controlling step. The addition of Ni remarkably enhanced the C–H activation over Ru in the lactic acid amination step and the transformation from glycerol to lactic acid. The optimized Ru<sub>1</sub>Ni<sub>7</sub>/MgO catalyst afforded value-added alanine directly from crude glycerol and is reusable. The novel reaction route from “waste” of the biodiesel plant to produce value-added amino acid adds new possibilities in biorefinery.

## Acknowledgements

This work was supported by the National University of Singapore Flagship Green Energy Program (R-279-000-553-646, and R-279-000-553-731). Q.H. thanks the support from the National Research Foundation, Singapore (NRF-NRFF11-2019-0002). XAS experiments was performed at a public beamline, BL01B1 at SPring-8 with the approval of JASRI (Proposal Nos. 2019A1447).

**Keywords:** Glycerol • Alanine • Ruthenium-Nickel • Heterogeneous catalysis • Amino acids

- [1] a) B. Katryniok, S. Paul, F. Dumeignil, *ACS Catal.* **2013**, *3*, 1819-1834; b) T. W. Walker, A. H. Motagamwala, J. A. Dumesic, G. W. Huber, *J. Catal.* **2019**, *369*, 518-525.
- [2] a) P. A. Jacobs, M. Dusselier, B. F. Sels, *Angew. Chem. Int. Ed.* **2014**, *53*, 8621-8626; *Angew. Chem.* **2014**, *126*, 8765-8770; b) C. Journoux-Lapp, K. De Oliveira Vigier, C. Bachmann, S. Marinkovic, B. Estrine, G. Frapper, F. Jérôme, *Green Chem.* **2017**, *19*, 5647-5652; c) X. Dai, S. Adomeit, J. Rabeah, C. Kreyenschulte, A. Bruckner, H. Wang, F. Shi, *Angew. Chem. Int. Ed.* **2019**, *58*, 5251-5255; *Angew. Chem.* **2019**, *131*, 5517-5517.
- [3] a) H. J. Kim, J. Lee, S. K. Green, G. W. Huber, W. B. Kim, *ChemSusChem* **2014**, *7*, 1051-1056; b) S. Lee, H. J. Kim, E. J. Lim, Y. Kim, Y. Noh, G. W. Huber, W. B. Kim, *Green Chem.* **2016**, *18*, 2877-2887; c) G. Dodekatos, S. Schünemann, H. Tüysüz, *ACS Catal.* **2018**, *8*, 6301-6333; d) P. N. Amaniampong, Q. T. Trinh, J. J. Varghese, R. Behling, S. Valange, S. H. Mushrif, F. Jérôme, *Green Chem.* **2018**, *20*, 2730-2741.
- [4] a) J. Ma, J. Song, H. Liu, J. Liu, Z. Zhang, T. Jiang, H. Fan, B. Han, *Green Chem.* **2012**, *14*, 1743; b) S. Wang, K. Yin, Y. Zhang, H. Liu, *ACS Catal.* **2013**, *3*, 2112-2121; c) D. Sun, Y. Yamada, S. Sato, W. Ueda, *Appl. Catal., B* **2016**, *193*, 75-92; d) Q. Sun, S. Wang, H. Liu, *ACS Catal.* **2017**, *7*, 4265-4275.
- [5] a) M. Dusselier, P. Van Wouwe, A. Dewaele, E. Makshina, B. F. Sels, *Energy Environ. Sci.* **2013**, *6*, 1415-1442; b) M. Morales, P. Y. Dapsens, I. Giovanazzo, J. Witte, C. Mondelli, S. Papadokonstantakis, K. Hungerbühler, J. Pérez-Ramírez, *Energy Environ. Sci.* **2015**, *8*, 558-567; c) N. Razali, A. Z. Abdullah, *Appl. Catal., A* **2017**, *543*, 234-246; d) Y. Shen, S. Zhang, H. Li, Y. Ren, H. Liu, *Chem. Eur. J.* **2010**, *16*, 7368-7371; e) T. Komanoya, A. Suzuki, K. Nakajima, M. Kitano, K. Kamata, M. Hara,

## COMMUNICATION

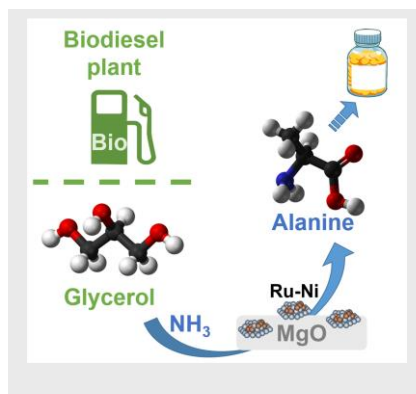
- ChemCatChem* **2016**, *8*, 1094-1099; f) Z. Jiang, Z. Zhang, T. Wu, P. Zhang, J. Song, C. Xie, B. Han, *Chem. Asian J.* **2017**, *12*, 1598-1604; g) A. M. Bruno, C. A. Chagas, M. M. V. M. Souza, R. L. Manfro, *Renew. Energ.* **2018**, *118*, 160-171; h) G. M. Lari, G. Pastore, M. Haus, Y. Ding, S. Papadokonstantakis, C. Mondelli, J. Pérez-Ramírez, *Energy Environ. Sci.* **2018**, *11*, 1012-1029; i) R. De Clercq, M. Dusselier, E. Makshina, B. F. Sels, *Angew. Chem. Int. Ed.* **2018**, *57*, 3074-3078; *Angew. Chem.* **2018**, *130*, 3128-3132.
- [6] G. Liang, A. Wang, L. Li, G. Xu, N. Yan, T. Zhang, *Angew. Chem. Int. Ed.* **2017**, *56*, 3050-3054; *Angew. Chem.* **2017**, *129*, 3096-3100.
- [7] a) V. M. Arredondo, P. J. Corrigan, *US 7,619,118 B2*, The Procter & Gamble Company, United States, **2009**; b) M. Ernst, B. W. Hoffer, J.-P. Melder, *US 2010/0240894 A1*, BASF SE, United States, **2010**, pp. 1-16; c) A. Venugopal, R. Sarkari, C. Anjaneyulu, V. Krishnaa, M. K. Kumar, N. Narender, A. H. Padmasri, *Appl. Catal., A* **2014**, *469*, 398-409; d) M. Safariamin, S. Paul, K. Moonen, D. Ulrichs, F. Dumeignil, B. Katryniok, *Catal. Sci. Technol.* **2015**, *6*, 2129-2135; e) X. Dai, J. Rabeah, H. Yuan, A. Bruckner, X. Cui, F. Shi, *ChemSusChem* **2016**, *9*, 3133-3138.
- [8] a) W. Deng, Y. Wang, S. Zhang, K. M. Gupta, M. J. Hülsey, H. Asakura, L. Liu, Y. Han, E. M. Karp, G. T. Beckham, P. J. Dyson, J. Jiang, T. Tanaka, Y. Wang, N. Yan, *Proc. Natl. Acad. Sci. USA* **2018**, *115*, 5093-5098; b) A. Afanasenko, T. Yan, K. Barta, *Commun. Chem.* **2019**, *2*, 127.
- [9] D. Li, I. Atake, T. Shishido, Y. Oumi, T. Sano, K. Takehira, *J. Catal.* **2007**, *250*, 299-312.
- [10] Z. Lu, I. Demianets, R. Hamze, N. J. Terrile, T. J. Williams, *ACS Catal.* **2016**, *6*, 2014-2017.
- [11] L. S. Sharninghausen, J. Campos, M. G. Manas, R. H. Crabtree, *Nat. Commun.* **2014**, *5*, 5084.
- [12] B. N. Zope, D. D. Hibbitts, M. Neurock, R. J. Davis, *Science* **2010**, *330*, 74-78.
- [13] P. Nash, *Bull. Alloy Phase Diagr.* **1986**, *7*, 130-133.

## COMMUNICATION

## Entry for the Table of Contents

## COMMUNICATION

**Direct conversion:** 43% alanine was achieved from crude glycerol over a  $\text{Ru}_1\text{Ni}_7/\text{MgO}$  catalyst. Ni-doped Ru remarkably promoted lactic acid amination, a key step in the reaction.



Yunzhu Wang, Shinya Furukawa, Song Song, Qian He, Hiroyuki Asakura, Ning Yan\*

Page No. – Page No.

Catalytic production of alanine from waste glycerol